Materials Research, Vol. 6, No. 4, 451-456, 2003.

Sb Doping Effects and Oxygen Adsorption in SnO_2 Thin Films Deposited *via* Sol-Gel

Viviany Geraldo[a], *Luis Vicente de Andrade Scalvi*[b]*, *Evandro Augusto de Morais*[a], *Celso Valentim Santilli*[c], *Sandra Helena Pulcinelli*[c]

[a]*Instituto de Física de São Carlos, USP*
C.P. 369, 13560-970 São Carlos - SP, Brazil
[b]*Departamento de Fisica - FC, UNESP*
C.P. 473, 17033-360 Bauru - SP, Brazil
[c]*Instituto de Química de Araraquara, UNESP*
C.P. 355, 14801-970 Araraquara - SP, Brazil

Received: January 29, 2003; Revised: August 31, 2003

Transparent electrically conducting antimony-doped SnO_2 thin films have been prepared by sol-gel dip-coating process from colloidal aqueous suspension. The effect of doping content on the structural, optical and electrical properties is analyzed. Results from infrared optical transmission and reflection have shown that the higher the Sb concentration the lower the transmission intensity and the higher the reflection signal. Absorption intensity increases as well. Results of X-ray reflectometry and electron microscopy have shown that the density of films fired at 400 °C after each dip is higher than that of multi-dipped films prepared with a single annealing. Both the electrical characteristics in the dark and the increase in conductivity as function of illumination through different filters, at 190 K, evidence that the transport properties of these films are dominated by the presence of defects, including the trapping at grain boundary due to excess of oxygen.

Keywords: *tin dioxide, nanostructures, sol-gel, optical properties*

1. Introduction

Tin dioxide is an n-type, wide bandgap semiconductor (about 3.5 eV) and in the form of thin films, it is a transparent conducting material, characterized by high optical transmission (80-90%)[1]. Optical, electrical and structural properties make tin dioxide very attractive for many kind of applications in opto-electronic devices[2], gas sensors[3-5] and solar collectors[6,7]. Moreover, doping tin dioxide with electronic donors as F^- or Sb^{5+} yields a high conductivity without significant changes in its optical transmittance[8]. Conducting SnO_2:Sb films exhibit increasing absorption coefficient in the infrared, where absorption spectra can be reasonably well described by Drude's free electron gas theory[9,10]. Transmission coefficient decreases with increasing thickness and doping levels[2], while reflection in the infrared region increases with increasing Sb concentration[10,11].

SnO_2 films properties are strongly influenced by preparation technique. The sol-gel process presents many advantages compared to other techniques, such as excellent homogeneity, thickness control and possibility of coating large and complex surfaces, using both inorganic and organic precursors, whereas alkoxids precursors are expensive and extremely sensitive to moisture, producing inhomogeneous layers when prepared under room atmosphere. The colloidal suspensions prepared via inorganic sol-gel route developed in our laboratory have been a preferred way to making SnO_2 films by dip coating, because these disadvantages are absent. But the electrical and optical properties of the layers prepared by sol-gel route are worse than those reported for films deposited by other techniques. The reasons for this worse performance are not completely understood yet, due to the difficulty to correlate the optical and electrical properties to the structural feature of the sol-gel films. This fea-

*e-mail: scalvi@fc.unesp.br
Trabalho apresentado no XV CBECIMAT, Natal - RN, Novembro de 2002.

ture is generally attributed to a combination of effects associated to the nanoscopic characteristic of sol gel materials, like reduced crystallite size, high porosity in combination with doping segregation and gas adsorption of gaseous species at the surface of the crystallites.

In this work, we present an analysis of the effect of Sb doping to polycrystalline SnO_2 thin films deposited via sol-gel route with several concentrations of Sb (1.5, 2, 3 and 4%) on their electrical and optical properties. In order to improve the film density and examine the effect of nanostructural feature on their optical and electrical properties, two distinct post-deposition annealing procedures were used, whose difference is basically a firing step at 400 °C between each dip.

2. Experimental

Colloidal suspensions of Sb-doped SnO_2 nanoparticles have been prepared from Sn^{4+} aqueous solution (0.25 mol/l), obtained by dissolution of $SnCl_4 5H_2O$ and SbF_3 (Merck). Hydrolysis was promoted by addition of ammonium hydroxide (NH_4OH) under magnetic stirring until pH reaches 11. The precipitate obtained by this way, was submitted to dialysis in order to eliminate as much as possible chloride, fluoride and ammonium ions. This procedure leads to stable SnO_2:Sb colloidal suspensions for several doping concentrations. These suspensions, were used for film deposition on silicate glass substrates by dip-coating technique, with a withdrawing rate of 10 cm/min. Multi-dipped films were deposited basically following two procedures, concerning firing between dips. They are described below:

Procedure I (PI) - After each dip, which takes place at room temperature, films are kept in air for 20 min and then dried in a oven at 50 °C by 30 min. When the desired number of layers is obtained, films are annealed at 500 °C for 1 h under air or vacuum.

Procedure II (PII) - the only difference to procedure I is that between each dip, the deposited film is fired at 400 °C for 10 min. In other words PII allows a significant increase on intermediate annealing temperature, which is carried out after each layer deposition.

Infrared transmittance and reflection have been measured by a Nicolet spectrophotometer in the range 1.8-12 μm. X-ray reflectometry measurements have been done in a reflection chamber coupled to a conventional powder diffractometer Siemens D5000, using CuK_α monochromatic radiation. The accuracy in the incident and detection angles was 0.001° and the width of both entrance and receiving slits were 0.01 mm to minimize the angular divergence. Simulation of experimental reflectivity curves has been done on the basis of the formalism developed by Nèvot-Croce[12] by means of the Refsimul software, developed by Siemens, which supplies the following structural parameters: i) apparent density, deduced from the critical angle; ii) thickness of the film deduced from the periodic oscillations and iii) interface roughness deduced from the amplitude of the periodic oscillations. To verify the thickness of multi-dipped films, scanning electron microscopy is carried out on samples with 50 dips, grown by both procedures. This is done with a Microscope Stereoscan 440-LEO.

To perform electrical measurements, In electrodes have been evaporated on the samples through a shadow mask in a Edwards evaporator system. Electrodes are annealed to 150 °C by 20 min in air. Low temperature electrical measurements were done in an Air Product Cryostat which controls temperature in the range of 25 to 300 K within 0.1 K of precision.

The average crystallite size has been determined from X-ray diffraction peaks, using Scherrer method[13], where the particle size decreases with half width increase. The broadening of half width is evaluated considering the contribution of grain size and due to instrument broadening[13].

3. Results and Discussion

3.1. Sb doping Influence on the infrared spectra

Figure 1 shows optical transmittance in the infrared of films prepared by both procedures. Main Fig. 1 shows the transmittance in the 2.4 to 5.4 μm range for samples obtained by procedure PII whereas inset of Fig. 1 shows infrared transmittance in the range 1.8 to 5.4 μm for PI films. In both cases the transmittance decreases as Sb concentration increases.

Figure 2 shows infrared reflection for PII films. Reflection increases with Sb concentration, in good agreement with transmittance data. Regions of lower transmittance are co-

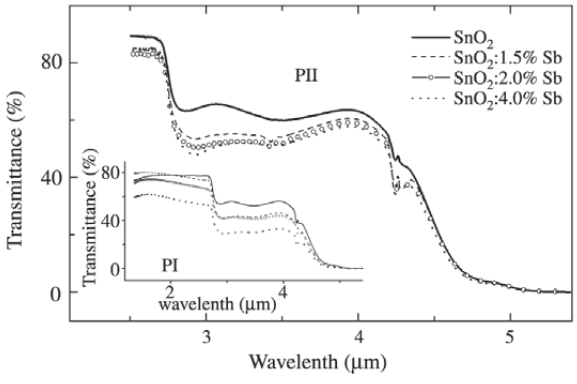

Figure 1. Near infrared transmittance spectra of SnO_2 thin films deposited by PII with several Sb doping composition. Inset - near infrared transmittance spectra of films deposited by PI.

incident with reflection maximum, meaning that the reflected fraction of the incident beam is probably more significant than absorption fraction in the infrared range. Small bands observed about 3.4 and 4.2 μm may be related to hydroxyl groups[14] that were not completely eliminated by annealing at 500 °C. Usually hydroxyl groups begin to be eliminated at 250 °C but they are not completely desorbed at 500 °C[15].

Evaluation of bandgap transition from optical absorption data in the ultraviolet to visible range yields an average value of 3.6 eV for indirect transition, in good agreement with expected energy (3.5-4.0 eV)[16].

In near infrared region the classical Drude theory applies, whenever the carrier concentration is high enough to allow plasma resonance phenomena. Then, reflection in infrared region increases with increasing Sb concentration. The plasma resonance frequency ω_p is given by[11]:

$$\omega_p^{\ 2} = (4 \pi N e^2).(\varepsilon_m \varepsilon_o m^*)^{-1} \quad (1)$$

N is the free electron concentration, ε_m and ε_o represent dielectric constants of medium and free space respectively and m^* is the effective mass of conduction band. The complex dielectric constant $\varepsilon(\omega)$ can be given by[17]:

$$\varepsilon(\omega) = 1 - \omega_p^{\ 2}/\omega^2 = 1 - \lambda^2 / \lambda_p^{\ 2} \quad (2)$$

where λ_p is the plasma resonance wavelength. If ε is real and negative ($\lambda > \lambda_p$), solutions of the wave equation decay exponentially so that no radiation can propagate through the film. Then a high reflection is expected. If e is positive ($\lambda < \lambda_p$), solutions become oscillatory and radiation can propagate. Estimation of free electron concentration from electrical resistivity data have yielded up to 5×10^{18} cm^{-3}, which would correspond to about 15 μm for λ_p. It means that the whole range shown in Fig. 1 and 2 are below the plasma resonance wavelength, and then, radiation should not be reflected. In order to describe the observed optical reflection in the infrared region of these films, concentration as high as 10^{20} cm^{-3} is needed[10,11]. The decreasing transmittance with increasing Sb concentration observed on films grown by both methods suggests that films may have indeed a high free carrier concentration in the neutral bulk region, but there is also a very high electron scattering at boundary layer. Sol-gel films used in our measurements have small grain size (3-10 nm) [18] and their resistivity is rather large. Then there is a large amount of crystallites concomitant with potential barrier at grain boundary which is related to large grain boundary depletion layer[19]. It leads to a strong electron scattering at grain boundary. Besides the presence of pores must be taken into account since it decreases the electron free path. Therefore the electron mobility of these sol-gel films is unusually low and it is responsible for the high resistivity observed in these films (see Fig. 5).

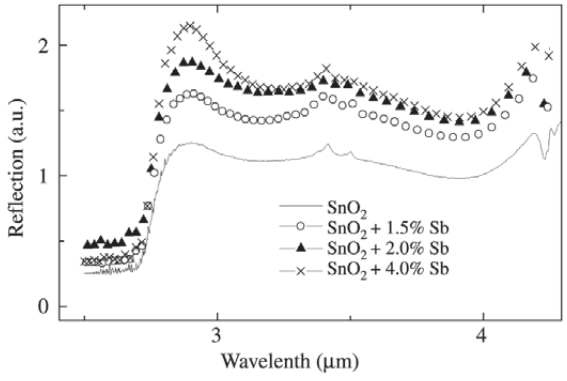

Figure 2. Near infrared reflection spectra for SnO_2:Sb thin films deposited by PII.

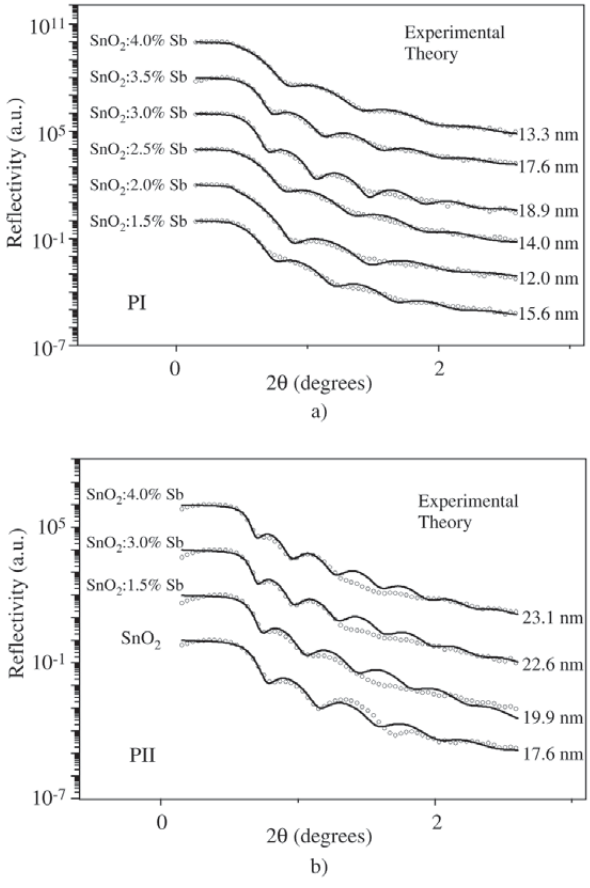

Figure 3. Experimental X-ray reflectivity curves (points) and fitted curves (lines) for Sb - doped SnO_2 films. a) films deposited by PI, single dip; b) films deposited by PII with 3 dips.

3.2. Influence of firing on SnO_2:Sb film deposition

Figure 3 shows the experimental X-ray reflectivity and fitted curves for samples obtained by PI and PII. Figure 3a shows results for single dipped films obtained by PI. The critical angle (θ_C), corresponding to total reflection, is invariant within experimental error, indicating that samples have the same density ($\cong 3.6 \pm 0.2$ g/cm^3). This low value indicates about 47% of pores when compared to SnO_2 single crystal. The periodicity of oscillation observed for $\theta > \theta_C$ indicates that films are continuous, presenting an uniform thickness. The film thickness, deduced from the period of oscillation, is in the range 12.0 nm to 18.9 nm, when Sb concentration is varied, even though no proportionality between thickness and Sb concentration is observed. Particularly for SnO_2:1.5%Sb films (composition used for MEV experiments - see next paragraph) the layer thickness is 15.6 nm. Figure 3b corresponds to X-ray reflectometry results and fitted curves for films obtained by PII. Films used in this case have 3 dips since 1 dip films obtained by this procedure turned out to be too thin and did not yield good simulation results. The density obtained from simulation parameters is about 4.7 ± 0.1 g/cm^3, which indicates a porosity of about 33%. These films also present continuous increase in thickness of 17.6 nm to 23.0 nm as the Sb content increases from 0.0 to 4.0%. Since these experimental curves correspond to films prepared with 3 dips, each layer of SnO_2:1.5%Sb film has average thickness of 6.6 nm.

Figure 4 shows scanning electron microscopy (SEM) results for SnO_2:1.5%Sb films prepared by both procedures, with 50 dips. As it can be seen, the film prepared by PI (Fig. 4a) is about 400 nm thick, whereas film prepared by PII is about 300 nm thick. A qualitative analysis indicates that SEM results agree with X-ray reflectometry results, which means that temperature of 400 °C for firing between dips (PII) decreases film thickness, since in both kinds of measurements PI yields thicker films than PII. The average thickness per dip calculated from these values are 8 nm and 6 nm for PI and PII, respectively. Then, a further comparison between results of SEM and X-ray reflectometry, yields that the agreement is much better for PII than PI, which suggests that using PII the structural feature of single dipped layer is essentially preserved after multiple dip. On the other hand, the thickness of each successive layer prepared by PI decreases as the number of dip application increases. This feature may be related to a higher porosity obtained from PI (47%), which suggests the existence of much more empty space, and a softer film which could either be more easily fulfilled by precursor solution or partially peeled during the upper layer application. As a consequence, it results in a non-homogeneous structure and a worse optical transmittance.

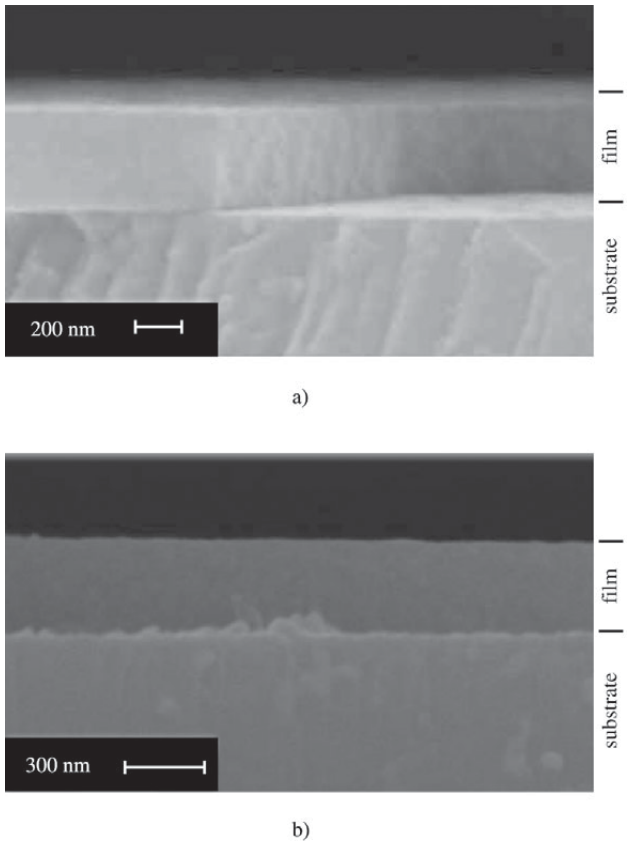

Figure 4. Scanning electron microscopy results to SnO_2 samples produced by a) PI; b) PII.

3.3. Electron trapping

Resistivity as function of temperature measured in the dark, for the range of 25 to 300 K is shown in Fig. 5 for a few films grown by procedure PII. The increase in the conductivity at 190 K for SnO_2:4%Sb film when submitted to tungsten light of 160 W, driven towards the region between contacts through a filter, is given in the inset of Fig. 5, whose cut-off wavelength is the x-axis. It is clearly seen that Sb doping increases n-type conductivity even though the resistivity is still rather high. It is interesting to mention that when SnO_2 films are annealed under vacuum its resistivity decreases. A similar film to that of Fig. 5 with 4%Sb, when annealed at 500 °C, under vacuum, presents resistivity of 9.3×10^{-3} ohm.m at room temperature. However this is not a permanent effect. Exposure to atmospheric air recovers the high resistivity. An Arrhenius plot of curves of Fig. 5 (not shown) yields activation energy of 144, 42 and 38 meV for the deepest level (ionized at higher temperature range) of undoped SnO_2, SnO_2:3.5%Sb and SnO_2:4.0%Sb respectively. The lower values are in good agreement with shal-

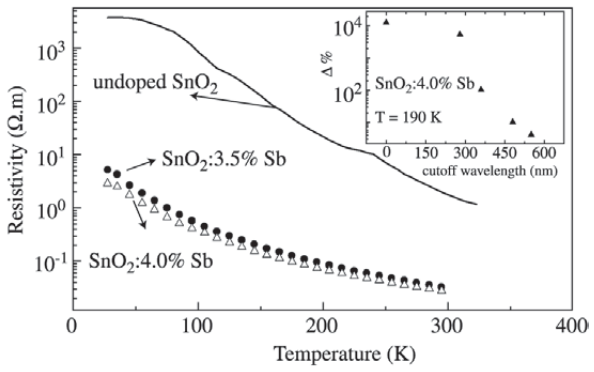

Figure 5. Resistivity as function of temperature for SnO_2 thin films prepared by PII, with 30 dips and 3 different Sb compositions. Inset - relative increase in the conductivity as function of illumination using filters with several different cut-off wavelengths, measured at 190 K.

low donor of antimony doping and the deeper one agrees with oxygen vacancy[20]. It is also interesting to mention that doubly ionized vacancies have also been taken as responsible for electron trapping in SnO_2 as published elsewhere[21]. In this case the values obtained could be related to first ionized state of oxygen vacancy (30 meV) and the deeper attributed to the second ionized level of oxygen vacancy[20]. Since our undoped sample does not present a shallower level about 30 meV, our conclusion is that 144 meV indeed corresponds to oxygen vacancy level and 38 to 42 meV are Sb donor ionization levels (slightly shifted with Sb concentration). The high resistivity observed in these films suggests the existence of another trapping level, which is not temperature dependent. The main effect of electron trapping in this defect is the increase of depletion layer around grain boundary, which decreases the mobility, and thus the conductivity. Sb donors that contribute to the conductivity are located in the very center of crystallites and are also responsible for infrared optical reflection as already discussed. The inset of Fig. 5 shows ionization of different levels inside the bandgap, so that when the bandgap transition is overcame (l_c < 280 nm) the conductivity is greatly increased (more than 1000% over the dark value). It is interesting to mention that this increased conductivity is "frozen" when illumination is removed. Only when the sample is heated, conductivity returns to room temperature value. This kind of measurement assures that there are states inside the bandgap which can be photoexcited. However it is difficult to associate them with the ionization energies obtained from Arrhenius plot, since deep level defects may show large Stokes shift, which is usually related to vacancy-like defects[22]. The high intensity of the excitation lamp also assures that either the concentration of these defects is small (the conductivity increases only a little) or they have photoemission energy very close to bandgap transition.

4. Conclusion

Infrared optical transmission of SnO_2 thin films, deposited by dip-coating via sol-gel, decreases with increasing Sb doping. This behavior can be explained based on Drude's free electron gas theory. In our films, reflection in the near infrared is due to a large amount of free electrons in the crystallite bulk region. In this case, the high resistivity is related to strong grain boundary scattering.

The firing process between each dip during deposition of SnO_2 thin films turned out to be responsible for a more compact arrangement of layers leading to more dense and thinner films concomitant with less pores. Besides this firing at 400 °C between dips promotes better agreement between X-ray reflectometry and SEM results, which means that as the number of dips increase, films submitted to intermediate annealing keep their thickness proportional to the number of deposited layers, whereas films with no firing between dips are subject to a shrinking as the deposition goes on.

Energy levels obtained from Arrhenius plot indicate the presence of vacancy-like defects. The low excitation with infrared illumination, and the increase of conductivity only close to bandgap transition suggest intra-bandgap trapping levels with large Stokes shift.

Although methods used here for sample preparation yields films with improved morphology and optical transmission, conductivity is still low and probably can be increased by elimination of excess of oxygen from grain boundary layer and other defects.

Acknowledgments

The authors wish to thank Prof. Ligia O. Ruggiero and Prof. Margarida J. Saeki for helping us with the technical setup. We also thank Brazilian financial sources for financial help: CAPES, CNPq, FAPESP and PRONEX.

References

1. Dien, E.; Laurent, J.M.; Smith, A. *J. European Ceramic Soc.,* v. 19, p.787, 1999.
2. Terrier, C.; Chatelon , J.P.; Roger, J. *A Thin Solid Films* v. 295, p. 95, 1997.
3. Guglielmi, M.; Menegazzo, E.; Paolizzi, M.; Gasparro, G.; Ganz, D.; Putz, J.; Aegerter, M.A. *J. Sol-Gel Sci. Technol.* v. 13, p. 679, 1998.
4. Nakata, S.; Ojima, N. *Sensors and Actuators B,* v. 56, p. 79, 1999.
5. Heilig, A; Barsan, N; Weimar, U; Gopel, W. *Sensors and Actuators B*, v. 58, p. 302, 1999.

6. Sanon, G; Rup, R; Mansingh, E.A. *Phys. Rev. B, vol.* 44, p. 5672, 1991.
7. Geoffroy, C.; G. Campet, G.; Merril, F.; Portier, J.; Salardenne, J.; Couturier, G. *Active and Passive Elec. Comp*., v. 14, p. 111, 1991.
8. zum Felde, U.; Haase, M.; Weller, H. *J. Phys. Chem. B*, v. 104, p. 9388, 2000.
9. Rockenberger, J.; zum Felde, U.; Tischer, M.; Troger, L.; Haase, M. ; Weller, H. *J. Chem Phys.*, v. 112, p. 4296, 2000.
10. Nutz, T.; Haase, M. *J. Phys. Chem. B*, v. 104, p. 8430, 2000.
11. Santhi, E.; Dutta, V.; Banerjee, A.; Chopra, K.L. *J. Appl. Phys.* v. 51, p.6243, 1980.
12. Nèvot, L.; Croce, P.; *Rev. Phys. Appl.,* v. 15, p. 761, 1980.
13. Cullity, B.D. *Elements of X-ray Diffraction*, Addson-Wesley Pub. Comp., Massachussetts, 1978.
14. Lin, Y.J.; Wu, C.S. *Surface Coatings Technology,* v. 88, p. 239, 1996.
15. Yamazoe, N.; Fuchigami, J.; Kishikawa, M.; Seiyama, T. *Surf. Sci*., v. 86, p. 335, 1979.
16. Kololuoma, T.; Rantala, J.T. *Electron. Lett.*, v. 36, p. 172, 2000.
17. Ashcroft, N.W.; Mermin , N.D. *Solid State Physics*, CBS Publishing, Philadelphia, p. 18, 1976.
18. Scalvi, L.V.A.; Messias, F.R.; Souza, A.E.; Siu Li, M.; Santilli, C.V.; Pulcinelli, S. H. *J. Sol-Gel Sci. Technol.*, v. 13, p. 793, 1998.
19. Messias, F.R.; Vega, B.A.V.; Scalvi, L.V.A.; Siu Li, M.; Santilli, C.V.; Pulcinelli, S.H. *J. Non-Crystalline Solids*, v. 247, p. 171, 1999.
20. Zarzebski, Z.M.; Marton, J.P. *J. Eletrochem. Soc,.* v. 123, p. 299C, 1976.
21. Samson, S.; Fonstad, C.G. *J. Appl. Phys.*, v. 44, p. 4618, 1973.
22. Lang, D.V.; Logan, R.A.; Jaros, M. *Phys. Rev. B*, v. 19, p. 1015, 1979.